Artifact-free calibration of spatial carrier interferometry

Brad Kimbrough, Korbinian Prause, Erik Novak

4D Technology Corporation, 3280 E. Hemisphere Loop, Suite 146, Tucson, AZ 85706
(520) 294-5600, (520) 294-5601 Fax, brad.kimbrough@4dtechnology.com

Spatial carrier interferometry is a well-known single frame wavefront phase measuring technique. In this technique a large relative tilt is placed between the test and reference beams producing a high frequency carrier fringe pattern which is modulated by the desired measurement wavefront. Implementation of spatial carrier interferometry is relatively easily accomplished on most advanced laser interferometers. Since it is a single frame technique, it provides robust vibration immunity, enabling measurements involving long paths or mechanically decoupled elements as well as metrology into vacuum chambers and overall environmental immunity. One of the major limitations of this technique is the degradation in measurement accuracy resulting from the large wavefront tilt applied between the test and reference beams. As a result of the large relative beam angle, the test and reference beams do not follow exactly the same path through the interferometer, resulting in what is generally known as retrace error. In this paper an automated calibration technique is introduced which determines the retrace error in a measurement setup without the use of a calibration artifact. This technique works well when measuring both flat and spherical test surfaces. In both cases, the difference between the calibrated wavefront and the wavefront measured on-axis with temporal phase shifting is less than .05 waves. This process allows nanometer-level measurement of precision optics even in difficult environments.

Keywords: Interferometer, Optical Testing, Spatial Carrier Interferometry, Interferometer Calibration

1. INTRODUCTION

Single frame interferometric measurement techniques provide a robust means of surface shape measurement in harsh vibration environments. Vibration immunity results from the ability to capture a measurement frame in a relatively short time period, typically less than 1 millisecond, enabling measurements involving long paths or mechanically decoupled elements as well as metrology into vacuum chambers. One of the most commonly used single frame technique involves the use of a linear spatial carrier, sometimes referred to as spatial carrier interferometry.[1] In this technique a large relative tilt is induced between the test and reference beams producing a high frequency carrier fringe pattern modulated by the desired measurement wavefront. Implementation of spatial carrier interferometry is relatively easily accomplished on most advanced laser interferometers. One of the major limitations of this techniques is the degradation in measurement accuracy resulting from the large wavefront tilt applied between the test and reference beams. As a result of the large relative beam angle, the test and reference beams follow different paths through the interferometer, resulting in what is generally known as retrace error. This error is especially significant when using high NA reference spheres. Can you give examples of the magnitudes?

In this paper an automated calibration technique is introduced which determines the retrace error in a measurement setup without the use of a calibration artifact. This technique works well when measuring both flat and spherical test surfaces. This paper begins with a background discussion on re-trace error and calibration techniques. Next, a detailed description of the proposed calibration procedure is provided. Finally, measurement results for both flat and spherical surfaces are given.

2. BACKGROUND

In general, any departure of the measured surface from that of the reference surface will result in a non-common return path through the interferometer, therefore producing some retrace error in the measurement.[2,3] This is true whether the measurement is on-axis as is the case from most temporal based phase measurements, or significantly off-axis as is the case for the linear spatial carrier technique. In the case of on-axis measurements of flat surfaces or spheres, retrace is minimized by nulling the interferometer. For non-planar or aspherical surfaces, nulling the interferogram is not an option and retrace must be accounted for if precision measurements are to be made. Evans proposed a technique to determine the retrace associated with non-zero fringe densities and it is his technique that motivated our work.[2] In his technique, a mapping of retrace error as a function of tilt is produced by making multiple measurements of a flat at various tilt angles in both the horizontal and vertical directions. A low order Zernike polynomial is then fit to each measurement and the coefficient of each polynomial term is plotted as function of tilt. In this way a calibration map is generated which provides the effect of measurement slope on each of the lower order Zernike terms. Measurement correction is then done as follows:

1. A measurement of the surface under test is made.
2. The local slope of the measurement is calculated.
3. The local slope values and the calibration map generated as discussed above is used to compute the aberrations that would be introduced into the full aperture if there was uniform slope equal to the measured slope across the full aperture.
4. For each point in the measurement field, the slope of induced aberration is computed.
5. Integration of the slope map produces a correction map that can be subtracted from the original data.

In the case of spatial carrier measurements, there is generally a significant relative tilt placed between the test and reference surfaces. The most common technique uses a tilt corresponding to a phase change of pi/2 per pixel in both the x and y directions. For example, a 1000 x 1000 pixel array would have 500 fringes at 45 degrees across the full sensor. For surfaces of modest to moderate departure, the retrace errors associated with surface shape are small compared to those resulting from the significant carrier tilt. Figure 1 shows the results of measuring a 4 inch flat in both temporal (on-axis) and spatial carrier mode. The measurements were made with a 4D Technology AccuFiz interferometer. The un-calibrated on-axis measurement has a peak to value figure of 0.039 waves, while the spatial carrier measurement shows a peak to valley shape of 0.095 waves.

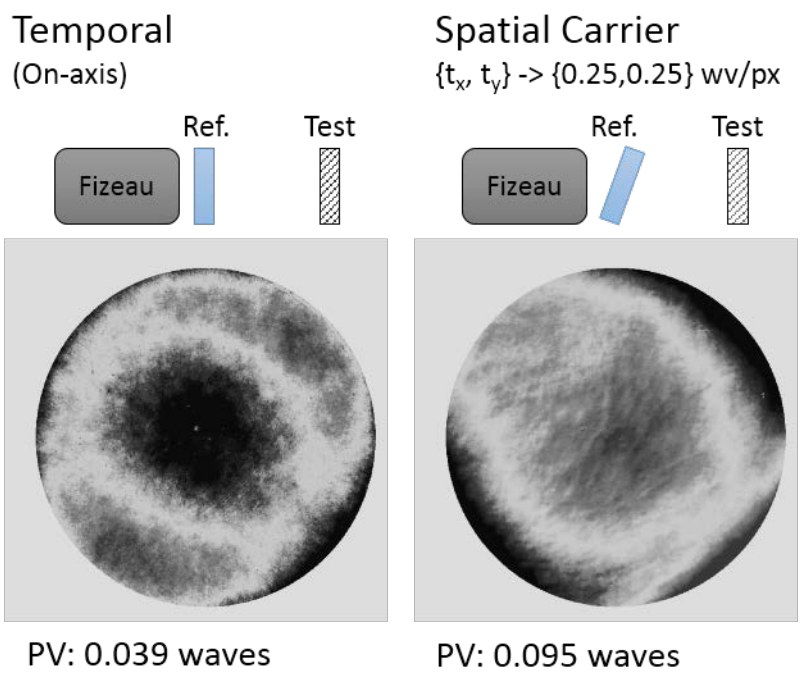

Figure 1. Temporal and spatial carrier measurement of a 4 inch flat. Both measurements were made using a 4D Technology AccuFiz interferometer

Due to retrace error the peak to valley surface height has more than doubled.

The most common calibration procedure for spatial carrier measurements utilizes a known measurement surface, sometimes called a calibration artifact. In this technique, the known surface is measured in spatial carrier mode. The difference between the measured surface and the known surface is the retrace error associated with the spatial carrier tilt. This error map is then used as the system reference and subtracted from subsequent measurements of other surfaces. Generally, an on-axis measurement of the artifact is made with a temporal measurement in order to produce the "known" surface, it is this measurement that is then subtracted from the spatial carrier measurement to produce the retrace error map.

Figure 2 shows the calculated error map obtained by subtracting the temporal measurement from the spatial carrier measurement of figure 1. As can be seen, the peak to valley surface shape of the calibration map is almost 4 times the on-axis value.

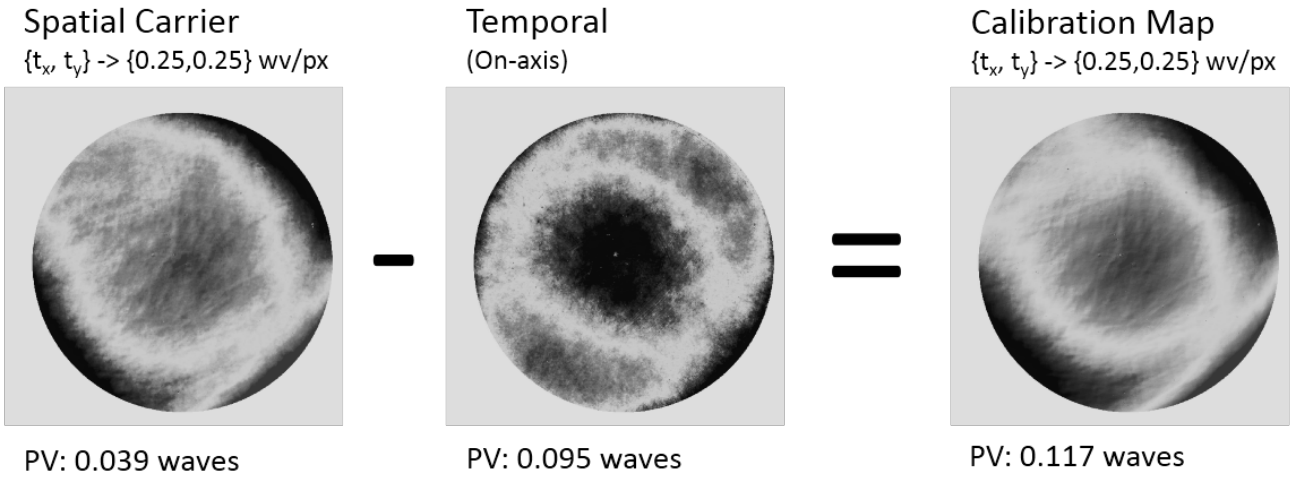

Figure 2. A calibration map for spatial carrier measurements is determined by subtracting the temporal measurement from the spatial carrier measurement of an artifact.

For most measurements, the use of a calibration artifact to determine a calibration map is relatively straightforward. However, there are situations where the use of a calibration artifact is not possible due to environmental factors, measurement arrangement, or cost. Referring to figure 2, if there were some way to estimate the on-axis measurement, then it would be possible to produce a calibration map without using a calibration artifact, and/or on-axis measurement. Building on Evans' technique, a procedure has been developed to estimate the on-axis measurement from a series of spatial carrier based off-axis measurements. This estimated on-axis measurement is then subtracted from a full spatial carrier measurement to obtain a calibration map for the system.

3. THEORY OF OPERATION

The proposed calibration technique assumes the following:

1. Any retrace error introduced due to the spatial carrier tilt will constitute a smoothly varying low order shape; representable by a 16 term Zernike polynomial series.

2. Plotting the value of a given Zernike polynomial term as a function of tilt results in a smoothly varying curve that may be interpolated at low order to determine the zero-tilt crossing point.

3. This technique only corrects for retrace error associated with the carrier tilt. It does not account for the measured surface contribution to retrace.

In the most general terms, the calibration technique determines the effect of tilt on the first 16 Zernike coefficients and uses this information to estimate what the coefficient of each of the 16 Zernike terms would be when the tilt value was at zero. In essence, a low order null surface is estimated.

The calibration technique is composed of the following steps:

1. A series of four spatial carrier measurements is made with full carrier, half carrier, -half carrier and –full carrier tilt fringes.

2. For each of the measurements a 16 term Zernike polynomial fit is calculated.

3. For each Zernike polynomial term, the four fit coefficients are plotted as a function of tilt. A third order polynomial fit of each Zernike term plot is then used to estimate the y-intercept (zero tilt) value.

4. The y-intercept point for each term is used to generate a reference null.

5. Finally, a calibration map is generated by subtracting the reference null from the Zernike fit of a full spatial carrier measurement.

3.1 Step 1: 4 Spatial carrier measurements

All measurements are done in single-frame spatial carrier mode. Two of the measurements are at +/- the full carrier tilt (pi/2 per pixel in both the x and y directions), the other two are at +/- half the full carrier tilt. In all cases the spatial carrier tilt was introduced by tilting the reference surface only. Figure 3 shows an example set of 4 measurements taken with a flat.

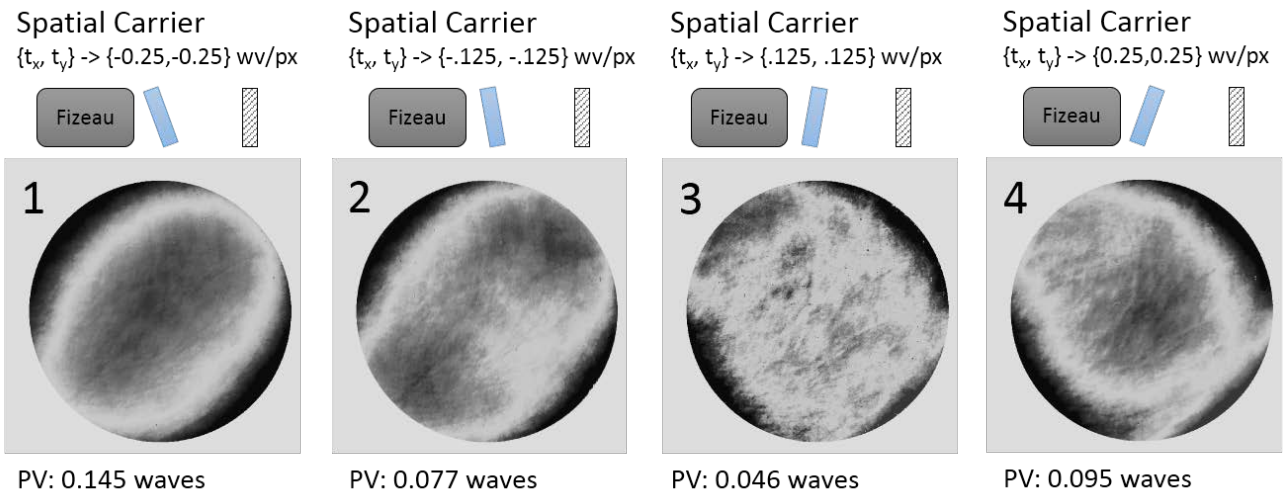

Figure 3. A series of 4 spatial carrier measurements. Measurement 1 is taken at full spatial carrier tilt at -135 degrees. Measurement two is at half of full spatial carrier tilt at -135 degrees. Measurement 3 is at half of full spatial carrier tilt at 45 degrees, and measurement 4 is a full spatial carrier tilt at 45 degrees.

3.2 Step 2: 16 Term Zernike fit

A 16 term Zernike polynomial fit is found for each of the 4 measurements. Table 1 provides the fit coefficients for the Z3 through Z8 terms for each measurements.

Table 1. Zernike coefficient values for measurements 1 through 4.

Measurement	1	2	3	4	Intercept
	(WV)	(WV)	(WV)	(WV)	(WV)
Z3 (Defocus)	-0.0565	-0.0297	-0.0027	-0.0153	-.0096
Z4 (Astig – X)	-0.0017	-0.0024	-0.0017	-0.0018	-.0022
Z5 (Astig – 45deg)	0.04	0.0286	-0.0099	-0.0197	.0091
Z6 (Coma X)	-0.0026	0.0003	-0.0018	0.002	-.0022
Z7 (Coma Y)	-0.001	-0.004	0.0008	-0.0048	-.0012
Z8 (Spherical)	-0.002	-0.0046	-0.0016	0.0024	-.0042

3.3 Step 3: Plot and Interpolate Zernike terms

For each of the Zernike terms, plot the 4 coefficient values as a function of tilt. Then fit a 3rd order polynomial to the points in order to determine the y-intercept which corresponds to the zero tilt or null value. Figure 5 shows the coefficient plots along with the 3rd order interpolation formulas for the Z3 through Z8 terms. The y-intercept is given by the constant term in each equation. This intercept value is also listed in the far right column of table 1.

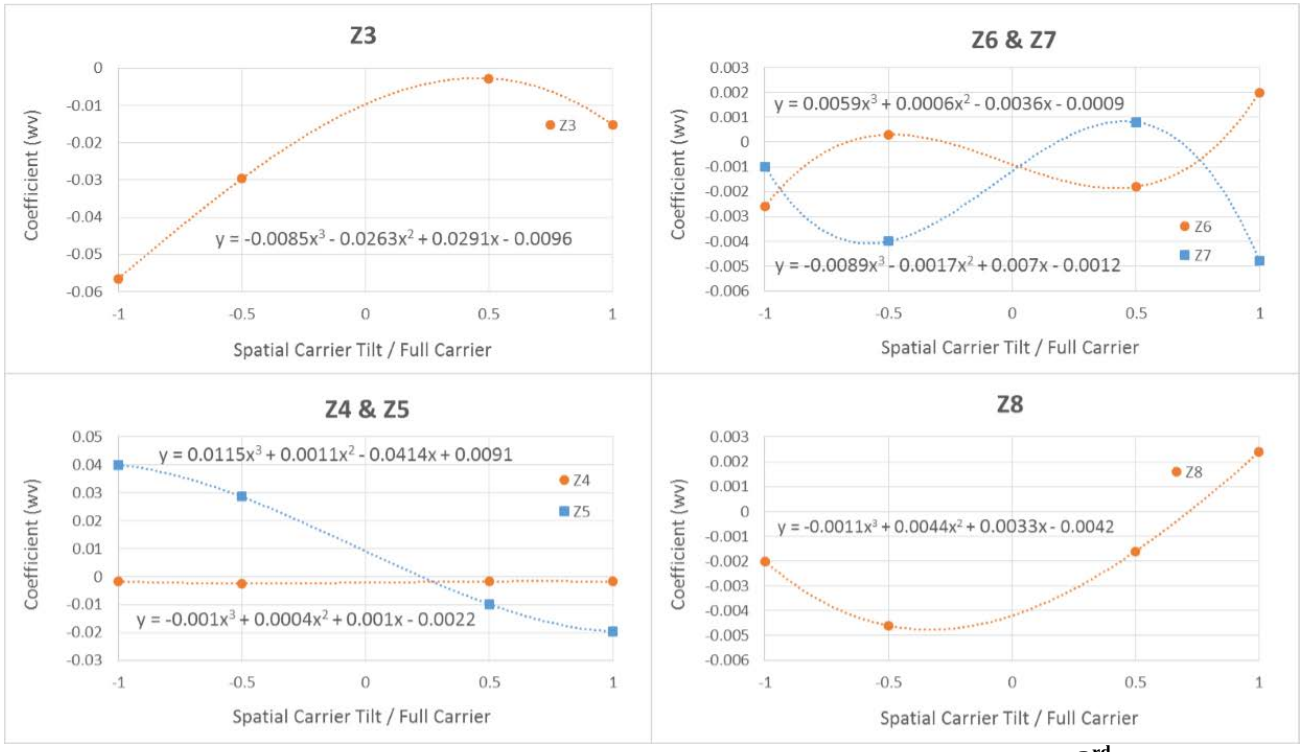

Figure 4. Zernike term coefficients as a function of spatial carrier tilt. For each of the plots, a 3rd order trend line is drawn and the associated polynomial is listed. The constant term in each polynomial corresponds to the estimated zero tilt value for each term.

3.4 Step 4: Generate the reference null

The reference null is generated as the sum of a 16 term Zernike polynomial where each polynomial coefficient is equal to the associated Zernike term zero tilt value found in step 3 above. The generated reference null along with a 16 term Zernike fit to the on-axis temporal measurement is shown in figure 5. It can be seen that the generated null is very close to the actual null measurement, with a difference RMS of 0.002 waves. The majority of this difference can be seen to be at the edges of the aperture.

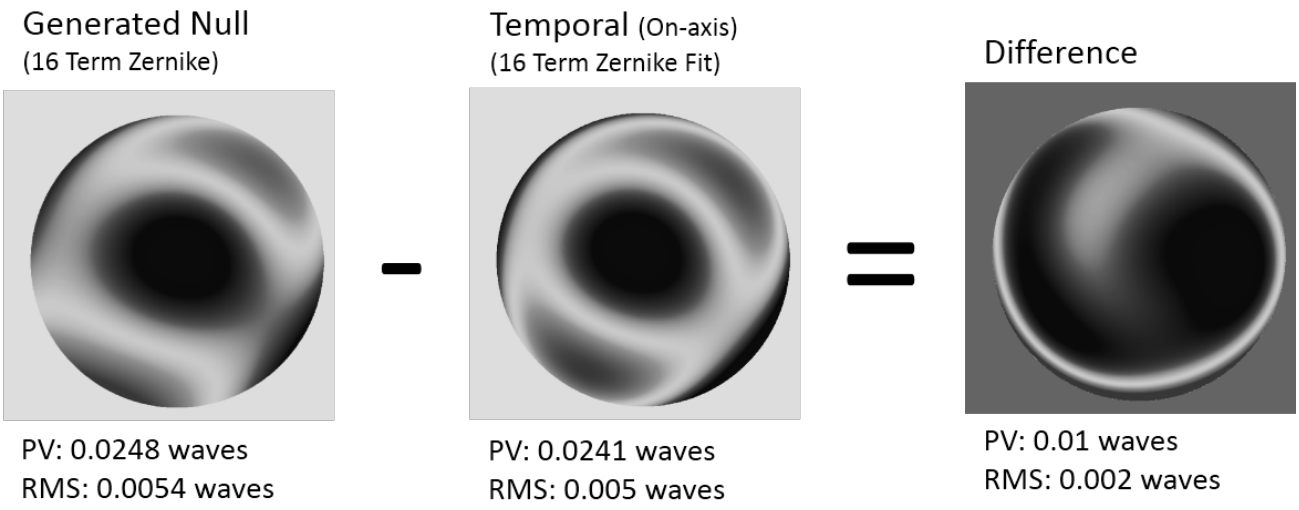

Figure 5. Comparison of the 16 term Zernike generated null with the measured on-axis null surface

3.5 Step 5: Generate the calibration map

A calibration map is generated by subtracting the generated null from a 16 term Zernike fit of the full spatial carrier measurement, measurement 4 of figure 3. This calibration map represents a 16 term Zernike approximation of the re-trace error associated with the spatial carrier measurement and can be used to correct any subsequent measurements made with the same spatial carrier tilt. Figure 6 shows the Zernike approximation of the full spatial carrier measurement along with the generated null and the resulting calibration map.

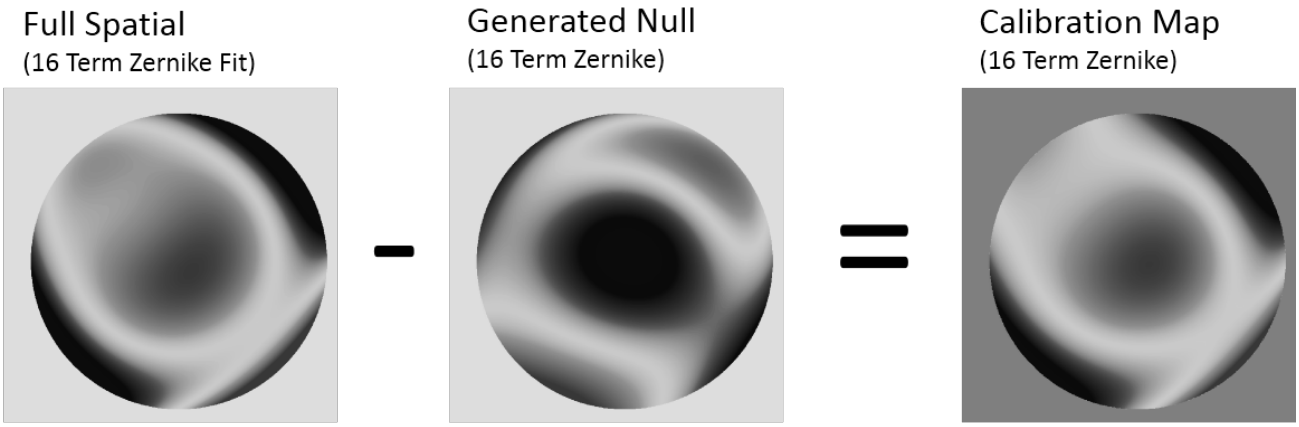

Figure 6. Calibration map generation. The calibration map is the difference of the 16 term Zernike fit of the full spatial carrier measurement and the generated reference null.

4. MEASUREMENT RESULTS

In order to demonstrate the performance of the calibration procedure outlined above, measurements were made of a flat, a spherical mirror with a f3.3 reference sphere, and a CaliBall with a f0.75 reference sphere. For comparison, each measurement was also done on-axis in temporal mode. All measurements were made with a 100mm 4D Technology AccuFiz interferometer. The AccuFiz interferometer is a laser based Fizeau interferometer with apertures ranging from 50 to 450mm. The calibration procedure was automated through the use of a motorized tip / tilt mechanism for the reference surface, and specialized control software. Once the system was aligned at null, calibration proceeded automatically, taking approximately 30 seconds to generate a reference surface using the procedure outlined above.

4.1 Flat Measurement

Figure 7 shows the results of the spatial carrier and temporal measurement of a flat surface. The difference between the calibrated spatial carrier measurement and the on-axis temporal measurement has an RMS of 0.004 waves. In addition to the low order shape seen in the difference measurement, there is also a higher order mottling of small amplitude. This mottling is also evident in the calibrated surface map, and is caused by beam shear in the interferometer. This same mottling is evident in a temporal measurement taken off-axis. In the absence of this shearing affect, the RMS difference between the calibrated spatial measurement and the temporal measurement would be 0.003 waves.

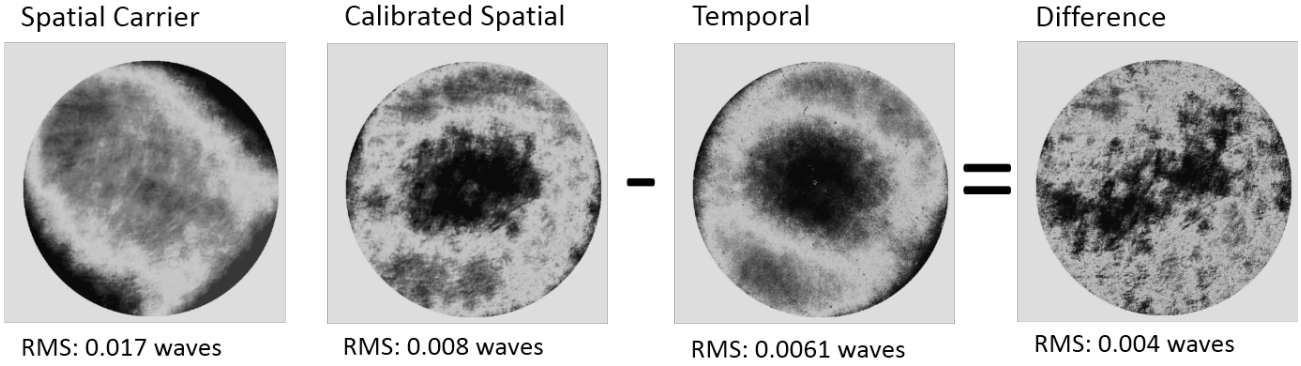

Figure 7. Calibrated spatial carrier measurement of a flat surface with comparison to on-axis temporal measurement.

4.2 Spherical surface measurement with an f3.3 reference sphere

Figure 8 shows the results of the spatial carrier and temporal measurement of a spherical surface with an f3.3 reference sphere. The difference between the calibrated spatial carrier measurement and the on-axis temporal measurement has an RMS of 0.003 waves. The mottling effect seen in the flat measurement is also evident. Although the RMS values between the calibrated and un-calibrated spatial carrier measurements are very similar, visually it is apparent that the wavefront shapes are quite different and that correction is necessary. An examination of the calibration wavefront would make this fact more evident.

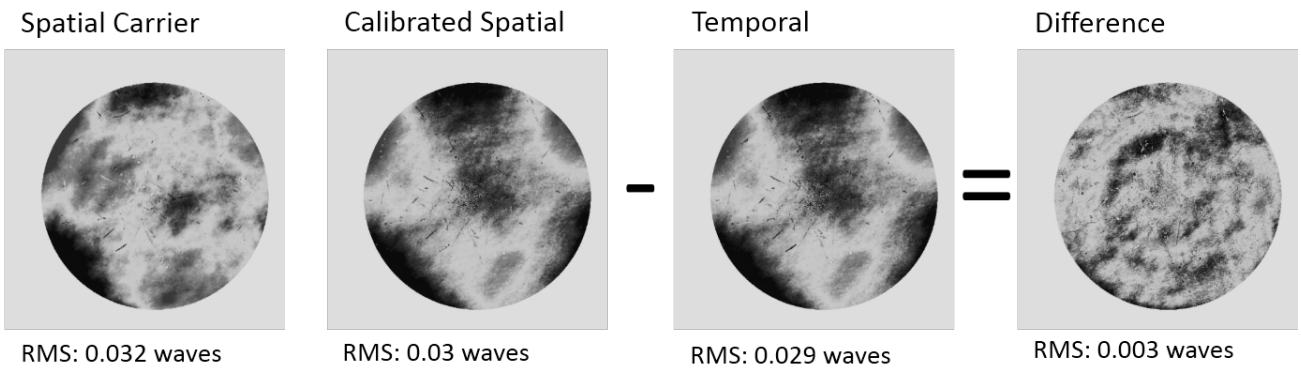

Figure 8. Spatial carrier measurement of a spherical surface using an f3.3 reference sphere with comparison to an on-axis measurement.

4.3 Spherical surface measurement with an f0.75 reference sphere

Figure 9 shows the results of the spatial carrier and temporal measurement of a CaliBall, a precision steel ball, with an f0.75 reference sphere. As can be seen, the spatial carrier measurement has significant retrace error, with a wavefront RMS more than 5 times that of the on-axis temporal measurement. Even so, the difference between the calibrated spatial carrier measurement and the on-axis temporal measurement has an RMS of only 0.016 waves, again demonstrating that it can correct the majority of errors associated with large tilts

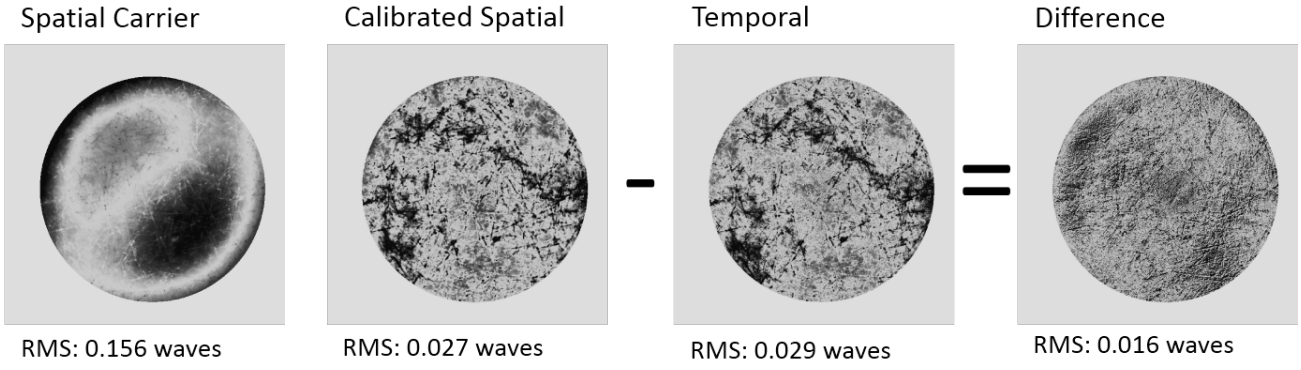

Figure 9. Spatial carrier measurement of a CaliBall using an f0.75 reference sphere with comparison to an on-axis measurement.

5. SUMMARY

Spatial carrier interferometry is a desirable interferometric technique in many situations where robustness to the environment is needed, enabling measurements involving long paths, mechanically decoupled elements, and into vacuum chambers. The many advantages of taking measurements in a single camera frame are however significantly offset by a decrease in measurement accuracy due to high relative tilts between the test and reference beams. This retrace error can be corrected, however, using a series of measurements taken at different relative tilts between the two beams. This technique has been automated in a commercially available laser-Fizeau interferometer. Various measurements on flat and spherical surfaces show that it corrects the majority of retrace errors, bringing the RMS difference between a corrected measurement and an on-axis temporally phase shifted measurement to below .016 waves even for very low numerical aperture measurements. Thus, nanometer-level measurement of precision optics is now possible even in difficult environments.

REFERENCES

1. D. Malacara, M. Servin, and Z. Malacara, “Interferogram analysis for optical testing,” (Marcel Dekker, New York, 1998).
2. C. J. Evans, “Compensation of errors introduced by non-zero fringe densities in phase measuring interferometers,” CIRP Annals 42/1, 577-580 (1993).
3. Andrew E. Lowman and John E. Greivenkamp, "Interferometer Errors Due to the Presence of Fringes," Appl. Opt. 35, 6826-6828 (1996).